HBRC Journal (2013) 9, 243–255

Housing and Building National Research Center

HBRC Journal

http://ees.elsevier.com/hbrcj

Characteristics of blended cements containing nano-silica

Mohamed Heikal [a,*], S. Abd El Aleem [b], W.M. Morsi [c]

[a] Chemistry Department, College of Science, Al Imam Mohammad Ibn Saud Islamic University (IMSIU), P.O Box 90950 Riyadh 11623, Saudi Arabia
[b] Chemistry Department, Faculty of Science, Fayoum University, Fayoum, Egypt
[c] Building Physics Institute BPI, Housing and Building National Research Center (HBRC), Dokki, Giza 11511, Egypt

Received 25 April 2013; revised 26 July 2013; accepted 11 September 2013

KEYWORDS

Granulated blast-furnace slag;
Nano-silica;
Hydration characteristics;
Blended cements;
Mechanical properties

Abstract The aim of the present work is to evaluate the effect of nano-silica (NS) on physico-chemical, compressive and flexural strengths of OPC-granulated slag blended cement pastes and mortars. Different mixes were made with various amounts of NS, OPC and granulated blast-furnace slag (GBFS) and hydrated for 3, 7, 28 and 90 days. The hydration behavior was followed by estimation of free lime (FL) and combined water content at different curing ages. The required water for standard consistency, setting times and compressive strength was also determined. The results obtained were confirmed by XRD, DTA, IR and SEM techniques. The required water for standard consistency and setting times increases with NS content due to the presence of 1% of superplasticizer. As the NS content increases the values of both FL and pH decrease. The compressive and flexural strengths of cement mortars containing NS are higher than those of control OPC–GBFS mix (M3). As the NS content increases above 4 mass% NS, compressive and flexural strengths of OPC–GBFS–NS blends decrease but still more than those of the control samples (M3). The results of XRD, DSC, IR and SEM examinations are in good harmony with each other and with chemical analyses. The composite OPC–GBFS–NS cements containing 45 mass% of GBFS and 3–4 mass% of NS possess the highest improvement of mechanical properties, hydration kinetics and microstructure of hardened cement pastes and mortars.

Introduction

Concrete is one of the most widely used construction material. However, the manufacture of Portland cement (main component of concrete) is highly energy intensive and involves the emission of CO_2 to the atmosphere. Nowadays, energy saving in building technology is one of the most important problems in the world. Reduction of energy usage can take place even by design methods [1] or using waste materials [2]. To save energy and reduce CO_2 emission, the mineral admixtures such as fly ash (FA), silica fume (SF), ground blast-furnace slag (GBFS) and metakaolin (MK)

* Corresponding author. Tel.: 00966122586751; mobile: 00966534484695; fax: 009662591678.
E-mail address: ayaheikal@hotmail.com (M. Heikal).

Peer review under responsibility of Housing and Building National Research Center.

Production and hosting by Elsevier

1687-4048 © 2013 Housing and Building National Research Center. Production and hosting by Elsevier B.V. All rights reserved.
http://dx.doi.org/10.1016/j.hbrcj.2013.09.001

are commonly used as a partial substitution of Portland cement. Also, these admixtures are often added to change the physical and chemical properties of the concrete [3–5].

GBFS has been used for many years as a supplementary cementitious material (SCM) in concrete, either as a mineral admixture or a component of blended cement. GBFS typically replaces 35–65 mass% of Portland cement in concrete. Thus 50 mass% replacement of Portland cement would result in a reduction of approximately 500,000 t of CO_2 over the world of cement production [6,7]. Using GBFS as a partial replacement takes advantage of the energy saving in Portland cement and is governed by AASHTO M302 [8].

Blast-furnace slag (BFS) is produced from the manufacture of pig iron. It forms when the slagging agents are added to the iron ore to remove impurities. In the process of reducing iron ore to iron metal, a molten slag forms as nonmetallic liquid that floats on the top of the molten iron. It is then separated from the liquid metal and cooled. Depending on the cooling mode, three types of slag are produced, i.e., air-cooled slag (ACS), expanded or foamed slag and granulated (sand-like) slag [9,10]. The rapid cooling of molten slag by water prevents the formation of large crystals, and the resulting slag normally contains more than 95% of glass (amorphous calcium aluminosilicates). This type of slag is called water-cooled slag (WCS) or granulated-blast furnace slag (GBFS) [6,11]. The chemical composition of slag can vary over a wide range depending on the nature of the ore, the composition of the limestone flux coke and the type of iron being made. The main constituents include: CaO, SiO_2 and Al_2O_3. In addition, it contains a small amount of MgO, FeO and sulfides such as CaS, MnO and Fe [12,13]. GBFS is widely used around the world as a cement replacement material in blended cements and shows both cementitious behavior and pozzolanic activity (reaction with free portlandite) [14,15]. Pure slag reacts with water at a slow rate. The presence of highly alkaline medium is required to disintegrate its acidic silicate–aluminate network [16–18].

Combining the management of wastes and nanotechnology can lead to accessing both performance of structural components and reduction of the harmfulness of hazardous byproducts. The application of nanotechnology in the civil engineering related industry can play an important role in the quality of building materials (strength, durability and lightness). Extremely fine size of nanoparticles (nPs) can greatly affect the hydration kinetics of cement, yielding favorable characteristics [19–25]. Nano-materials (NMs) show unique physical and chemical properties than ones, which are currently available [26–28]. The tendencies to agglomerate of NMs can be restricted by using dispersing admixtures or by applying different techniques during the mixing process [29,30]. NMs improve the performance of cement; in fresh or in hardened state, where the strength properties were increased as well as promote the hydration reactions [31–34].

The most commonly used NMs in cement products are nano-SiO_2 (NS), TiO_2 (NT), Al_2O_3 (NA), Fe_2O_3 (NF), ZnO (NZ) and carbon nano-tubes (CNTs) [35–43]. NS has a significant role, due to the highly pozzolanic activity with calcium hydroxide (CH) released during the hydration of cement phases to form more hydrated products, which fill the available pores with improving the microstructure [44–48]. Senff et al. [33] found that, fluidity; spreading and hardening time of the cement paste and mortar were reduced as the NS content was increased. In general, the presence of NS accelerates the initial hydration of C_3S as a result of its highly reactive surface [33,49,50]. As a consequence, the microstructure becomes more closed and compact, hence mechanical properties are improved [51–53].

Using slag in cement pastes, mortars and concretes as a binder has been addressed in several works, but there are few articles related to the impact of nano-particles on the hydration characteristics and microstructure of blended cements containing slag. Therefore, this study aims to investigate the characteristics of blended cements containing nano-SiO_2 and GBFS.

Materials and methods

Materials

The starting materials used were ordinary Portland cement (OPC), granulated blast-furnace slag (GBFS), nano-silica (NS) and polycarboxylate superplasticizer. OPC was provided by Beni-Suief Portland Cement Company and GBFS was supplied from the Iron and Steel Company, Helwan, Egypt. Their chemical analyses are given in Table 1. The Blaine surface area of OPC and slag were 3050 and 4000 cm^2/g, respectively. Nano-silica with the average particle size of 15 nm, 99.9% purity was supplied from the nano-technology laboratory, Faculty of Science, Beni–Suief University, Beni–Suief, Egypt. XRD, TEM and SEM of NS are given in Figs. 1 and 2. Conplast SP 610 superplasticizer was obtained from Fosroc Company, 6 October City, Egypt. It is an opaque light yellow liquid with density 1.08 g/ml and chloride content < 0.1 mass%.

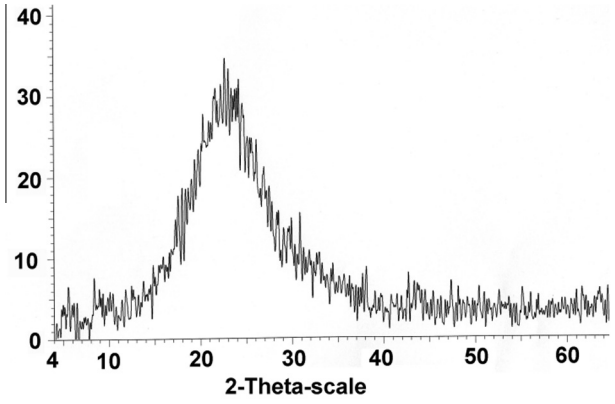

Fig. 1 XRD of nano-silica.

Table 1 Chemical analysis of OPC (mass%).

	SiO_2	Al_2O_3	Fe_2O_3	CaO	MgO	SO_3	Na_2O	K_2O	L.O I.	Total
OPC	21.30	3.58	5.05	63.48	1.39	2.05	0.26	0.22	2.57	99.90
Slag	43.21	9.97	0.59	35.96	5.43	1.37	0.79	0.67	1.98	99.97

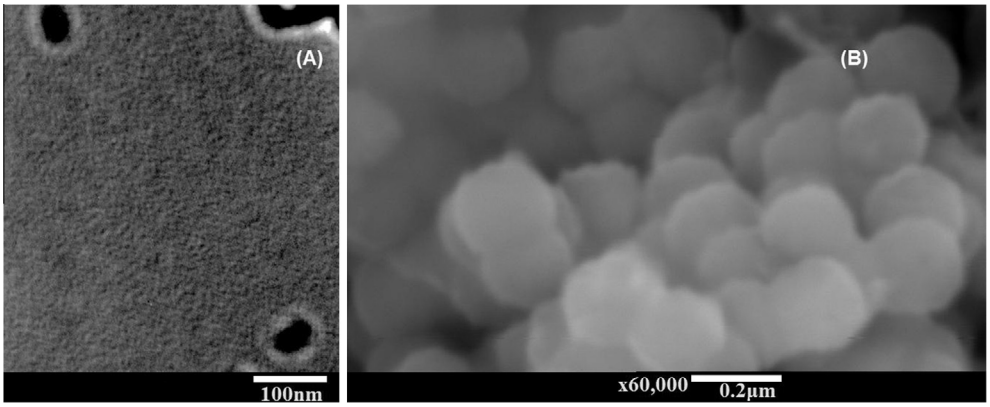

Fig. 2 (A) TEM and (B) SEM photographs of NS.

Methods

The cement blends were mixed in a rotary mixer according to the following sequence: (i) NS was stirred with 1.0% superplasticizer and 25% of mixing water at a high speed of 120 rpm for 2 min, (ii) the cement and the residual amount of mixing water were added to the mixer at medium speed (80 rpm) for 1 min, (iii) the mixture was allowed to rest for 90 s and then mixed for 1 min at high speed. For preparation of the mortars, the sand was added gradually and mixed at a medium speed for an additional 30 s after step (ii). The mortars were prepared by mixing 1 part of cement and 2.75 parts of standard sand proportion with water content to obtain a flow of 110 ± 5 with 25 drops of the flowing table [54]. Freshly prepared cement mortars were molded in $50 \times 50 \times 50$ mm cubic molds. The molds were vibrated for few minutes for better compaction. The mix compositions of the prepared cement blends are given in Table 2.

The required water of standard consistency and setting times was measured according to ASTM specification [55]. The hydration of cement pastes was stopped as described in a previous work [56]. The chemically combined water (W_n) and free lime (FL) contents were determined elsewhere [57,58]. The pH values of hardened cement paste were measured by placing about 10 g of the ground dried specimen into 100 ml of distilled water, then stirring for 30 min using a magnetic stirrer, and then the pH value was measured using pH meter,

Table 2 Mix composition of OPC and blended cements, mass%.

Mix no.	OPC	GBFS	NS
M0	100	0	0
M1	85	15	0
M2	70	30	0
M3	55	45	0
M4	40	60	0
M5	54	45	1
M6	53	45	2
M7	52	45	3
M8	51	45	4
M9	50	45	5
M10	49	45	6

Schott. GLAS Mainz-type CG 843-Germany. Bulk density [58], and compressive strength were measured according to ASTM (Designation: C-150, 2007) [59]. Some selected hydrated samples were investigated using XRD, FTIR, DSC and SEM techniques. For XRD, a Philips diffractometer PW 1730 with X-ray source of Cu K_α radiation (λ = 1.5418 Å) was used. The scan step size was 2θ in the range from 5° to 65° at collection time 1 s. The X-ray tube voltage and current were fixed at 40 kV and 40 mA, respectively. An on-line search of a standard database (JCPDS database) for X-ray powder diffraction pattern enables phase identification for a large variety of crystalline phases in a sample [60]. FTIR spectroscopic analysis was carried using a Mattson Gensis IR spectrometer in the range from 400 up to 4000 cm^{-1} [61]. DSC was conducted using Shimadzu DSC-50 thermal analyzer at a heating rate of 10 °C/min. with nitrogen at a flow rate of 30 cm^3/min. The microstructure was investigated by ESEM "Inspect S", FEI Holland. Backscattered electron detector (BSED) imaging was used to study the specimen's morphology without any coating.

Results and discussion

Characteristics of OPC–GBFS blends

The variations of the required water of standard consistency as well as setting times of the prepared cement pastes made of OPC and OPC–GBFS mixes (M0, M1, M2, M3 and M4), are graphically represented in Fig. 3. It can be seen that the water demand decreases and setting times increase with increasing the slag content. This is due to the lower hydraulic reactivity of GBFS in comparison with OPC during the very early ages of the hydration; this is due to the formation of acidic oxide film formation on the outer most layers of slag grains, which hinder the water penetration and the progress of hydration reaction at the very early ages of the hydration [62].

The chemically combined water content (W_n, %) of the hydrated OPC and OPC–GBFS pastes are graphically represented as a function of curing time in Fig. 4. W_n% increases with curing time for all hydrated cement pastes, this is mainly due to the increase of the amount of hydrated products in addition to the reaction of the slag portion with $Ca(OH)_2$, which precipitated in open pore systems [63]. The OPC–GBFS cement pastes give relatively lower combined water content than those of OPC, especially at early hydration

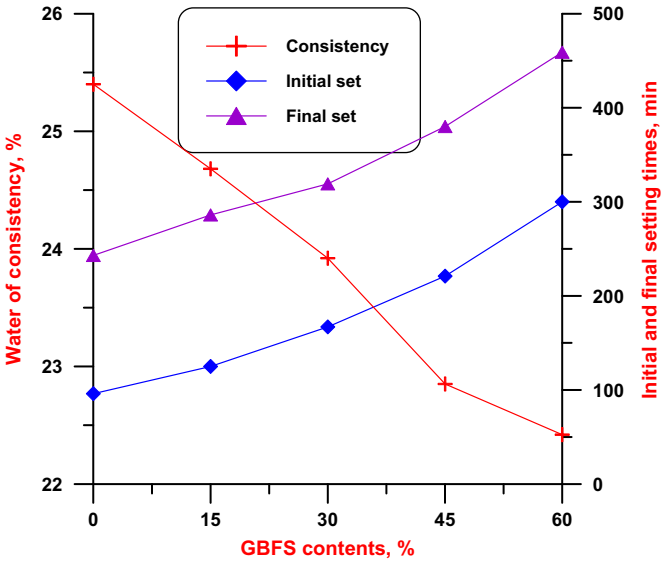

Fig. 3 Water consistency, initial and final setting times of the investigated cement pastes.

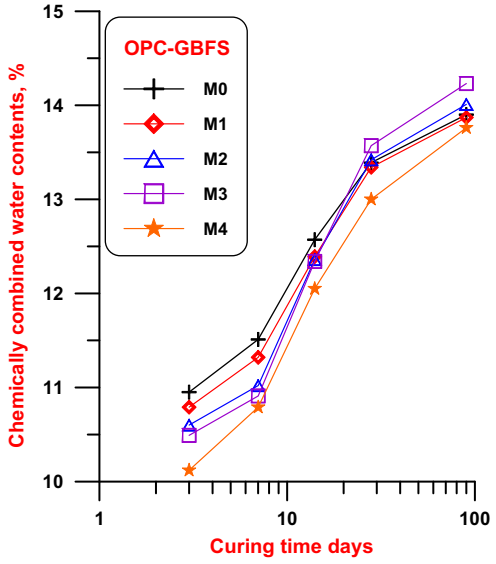

Fig. 4 Combined water content of hydrated cement mixes containing GGBFS with curing time up to 90 days.

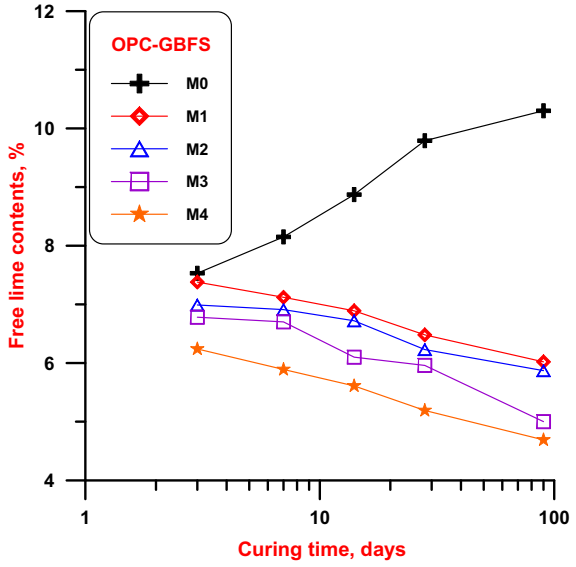

Fig. 5 Free lime contents of cement pastes containing different slag portions hydrated up to 90 days.

ages up to 14 days. But, at later stages of the hydration, cement mixes M_2 and M_3 show higher values of chemically combined water content than those of OPC; this is attributed to the higher pozzolanic activation of slag portion at longer curing times.

The pozzolanic reaction of GBFS can be followed by monitoring the values of pH and/or free lime (FL%) content of OPC–GBFS cement pastes at different hydration times up to 90 days. FL% and pH value of the investigated cement pastes are graphically plotted as a function of curing time in Figs. 5 and 6, respectively. The results of Figs. 5 and 6 indicate that the values of FL and pH decrease with increasing hydration time for all OPC–GBFS cement pastes, whereas the values of pH and free lime content of the neat OPC paste increase with the increasing of curing time up to 90 days. This is due to the hydration progress of OPC cement pastes with a continuous liberation of free $Ca(OH)_2$. On the other hand, FL% of OPC–GBFS cement pastes decreases with increasing slag content.

There are two opposing processes, the first is the hydration of cement clinker phases (lime production) and the second is the pozzolanic reaction of GBFS with the liberated free $Ca(OH)_2$ (lime consumption). The rate of the second process exceeds that of the first process, especially at the later hydration times. The increase of GBFS content decreases the values of the FL and pH, due to the decrease in the content of OPC (dilution effect).

The variations of bulk density (dp), compressive and flexural strengths of the hydrated OPC–GBFS blended cement mortar are plotted as a function of curing time up to 90 days in Figs. 7–9, respectively. It is clear that, the compressive and flexural strengths as well as the bulk density increase with

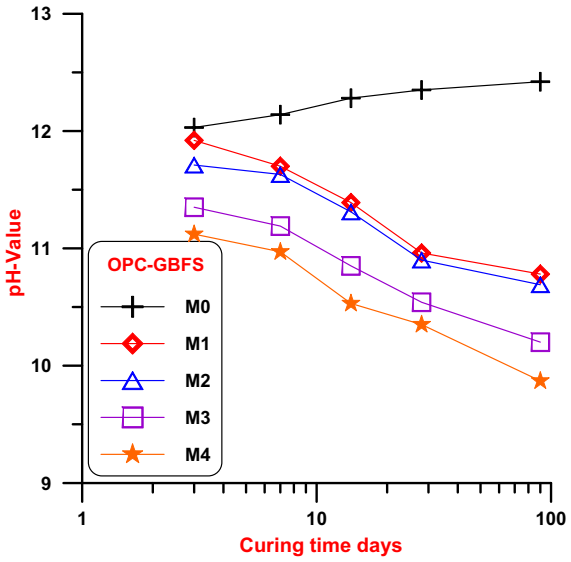

Fig. 6 pH-values of cement pastes containing different slag portions and hydrated up to 90 days.

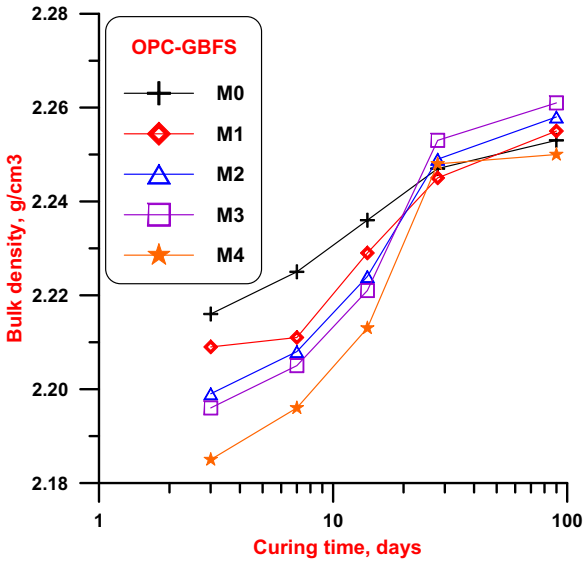

Fig. 7 Bulk density of hardened cement mortars containing different GBFS contents hydrated up to 90 days.

the increase of the curing time for all blended cement mortars; this is due to the continuous hydration and formation of hydrated calcium silicate (CSH), aluminate (CAH) and alumino-silicate (CASH) hydrates, which precipitate in the open available pores, leading to the formation of more homogeneous and compact structure. The compressive and flexural strengths decrease with increasing GBF content at early hydration ages. The values of compressive and flexural strengths of OPC–GBFS blended cement mortar are higher than those of the OPC mortar; this is due to the pozzolanic reaction of GBFS with the liberated CH from OPC cement hydration, which enhances at later hydration times [64,65], leading to the formation and accumulation of additional CSH, CAH and CASH hydrates, which are responsible for strength properties. By increasing GBFS content (M3) the values of compressive and flexural strengths exceed those of the values of control OPC mix. On the other hand, M4 that contains 60 mass% of GBFS has lower strength properties than OPC mortar up to 90 days. It has been found that, 45 mass% of GBFS as a partial replacement of OPC has the optimum mix composition.

Fig. 10 shows XRD patterns of the blended cement paste made of M3 hydrated up to 90 days. Evidently, the hydration products are mainly calcium silicate hydrate (CSH) with various C/S ratios and portlandite (CH) in addition to the remaining anhydrous parts of β-C_2S and C_3S grains. As the hydration proceeds, the peak intensity of CSH increases, whereas those peaks of CH decrease; this is due to pozzolanic reaction of the active silica and alumina of the GBFS with the released portlandite during OPC cement hydration.

FTIR spectra of OPC–GBFS cement paste containing 45 mass% of GBFS (M3) hydrated at different times are graphically represented in Fig. 11. Evidently, Fig. 11 shows a small peak located at about 3650 cm^{-1} due to –OH group from $Ca(OH)_2$ [66]. The intensity of this peak decreases with curing

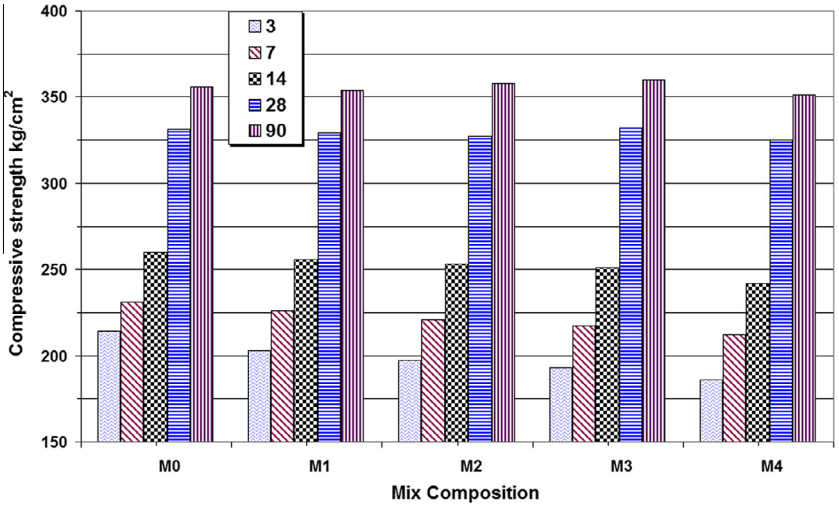

Fig. 8 Compressive strength of hardened cement mortars containing different GBFS contents hydrated up to 90 days.

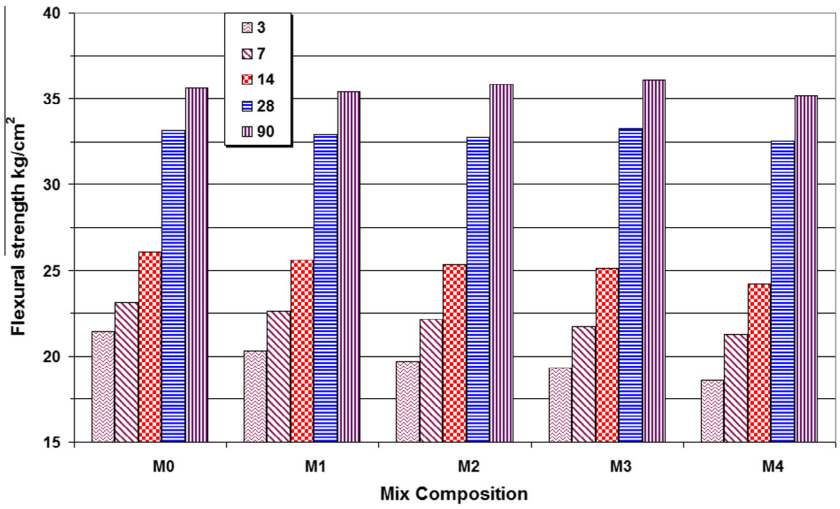

Fig. 9 Flexural strength of hardened cement mortars containing GBFS with curing time up to 90.

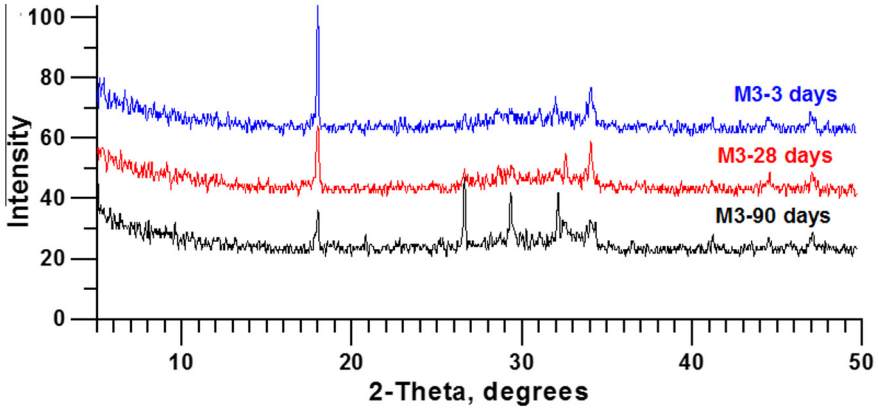

Fig. 10 XRD patterns of blended cement paste of M3 hydrated at 3, 28 and 90 days.

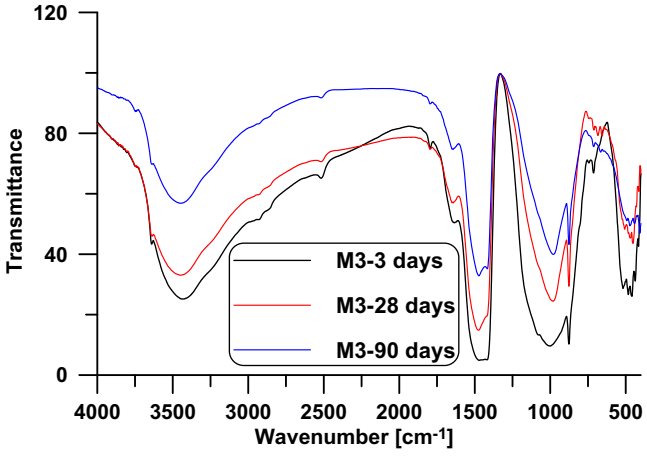

Fig. 11 FTIR spectra of hydrated M3 at different curing times.

time, due to the pozzolanic activity of slag. The broad bands located at 3400 and 1640–1650 cm^{-1} are assigned to the stretching and bending vibrations of water lattice in CSH, CAH and CASH hydrates. The band that appeared around 950 cm^{-1} is attributed to CSH [67]. Its intensity increases with curing time, due to the continuous hydration of OPC phases as well as the pozzolanic reaction of slag portion with free portlandite. The observed band at 1475 cm^{-1} is due to the stretching vibration of C–O bond in CO_3^{2-}, which results from the carbonation of hydrated products. Its intensity decreases with curing time, due to the increase of bulk density and the hindrance of carbonation of the hydrated samples. The observed bands at about 1080 and 485 cm^{-1} may be due to SO_4^{2-} associating with ettringite formation, which decreases with curing time, due to the increase of hydration activity of slag and formation of more CSH instead of hydrated calcium sulfoaluminates.

Fig. 12 represents the DSC thermograms of M3 cement paste hydrated at 3, 28 and 90 days. The following peaks are observed: (i) an endothermic peak in the temperature range of 80–120 °C related to the removal of free water as well as the dehydration of CSH, aluminate and sulfoaluminate hydrates, which clearly increases in intensity with hydration time; (ii) an endothermic peak at temperature of 485 °C, which is attributed to the $Ca(OH)_2$ decomposition, which decreases in intensity with increasing hydration time, indicating the progress of pozzolanic reaction (consumption of $Ca(OH)_2$ by

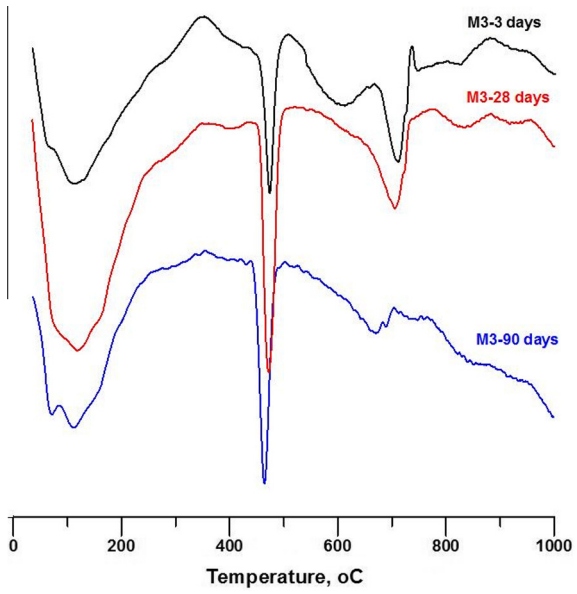

Fig. 12 DSC thermograms of M3 cement paste with curing times up to 90 days.

GBFS); (iii) an endothermic peak at the temperature range 700–760 °C attributed to the decomposition of $CaCO_3$. The intensity of hydrated calcium silicate peak increases with increasing time of the hydration.

Characteristics of OPC–GBFS–NS blends

Water of standard consistency and setting times of OPC–GBFS–NS composite cement pastes as a function of NS content are graphically illustrated in (Fig. 13). It is evident that the water of standard consistency increases with NS content. The increase of water of standard consistency may be due to high fineness and surface area of NS [49,68]. Setting times are elongated with NS content. The retardation of the setting processes is due to the presence of 1% of polycarboxylate superplasticizer as well as the excess of mixing water required for standard consistency [24,49].

Fig. 14 shows the chemically combined water content (Wn,%) of hydrated cement pastes up to 90 days. The results of W_n contents reflect the increase in hydration reaction rate for OPC–GBFS–NS composite cement pastes containing nano-particles. The values of W_n increase with increasing NS content. Nano-SiO_2 reacts with liberated $Ca(OH)_2$ from the hydration of OPC to form additional hydrated products (CSH, CAH and CASH). Also, NS particles accelerate the hydration of cement, due to their high activity and nucleating effect [49,69]. The composite cement containing 3 mass% of NS (M3) has the highest values of W_n, especially at later ages of hydration.

The variations of free lime contents (FL%) and pH values of cement pastes containing different percentages of NS hydrated up to 90 days are graphically shown in Figs. 15 and 16 respectively. It is obvious that, FL% and pH values decrease with curing time for all cement pastes, this is due to the pozzolanic reaction of both GBFS and NS with the liberated free portlandite from the hydration of OPC clinker phases (β-C_2S and C_3S) [24]. As the nano-SiO_2 content increases, the values of both FL and pH decrease, due to the higher pozzolanic affinity of NS in comparison with GBFS.

Figs. 17–19 represent the variations of compressive and flexural strengths and bulk density (dp) of the hydrated composite cement mortars as a function of NS content up to 90 days. The results indicate that the compressive and flexural strengths and bulk density are improved with age, due to the effect of NS, leading to the formation and accumulation of excessive amounts of hydrated products mainly as CSH, which fill the pore system and tend to increase the gel/space ratio, causing packing effect [55]. The compressive and flexural strengths of cement mortars containing NS are higher than those of the control OPC–GBFS sample (M3). The results also show that the compressive and flexural strengths and bulk density of the investigated specimens increase with NS up to 6%.

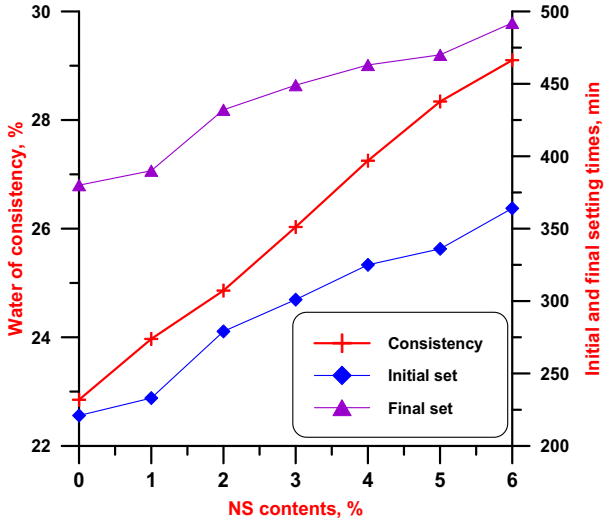

Fig. 13 Water consistency, initial and final setting times of OPC–GBFS–NS pastes as a function of nano-silica content.

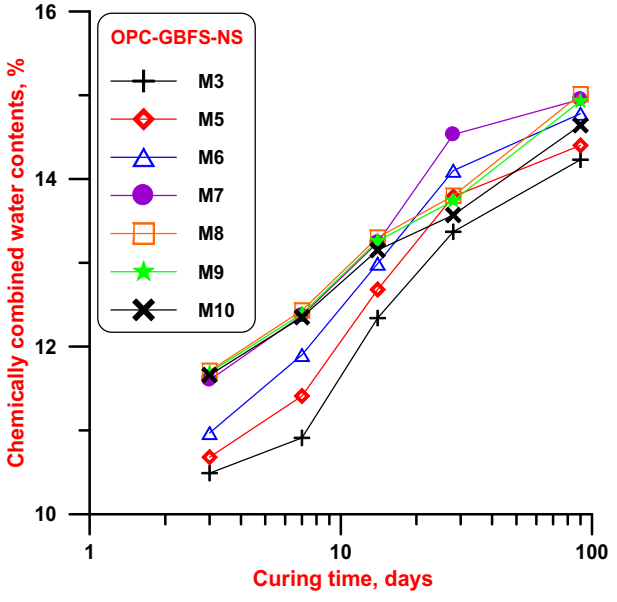

Fig. 14 Combined water content of cement mixes containing different NS% hydrated up to 90 days.

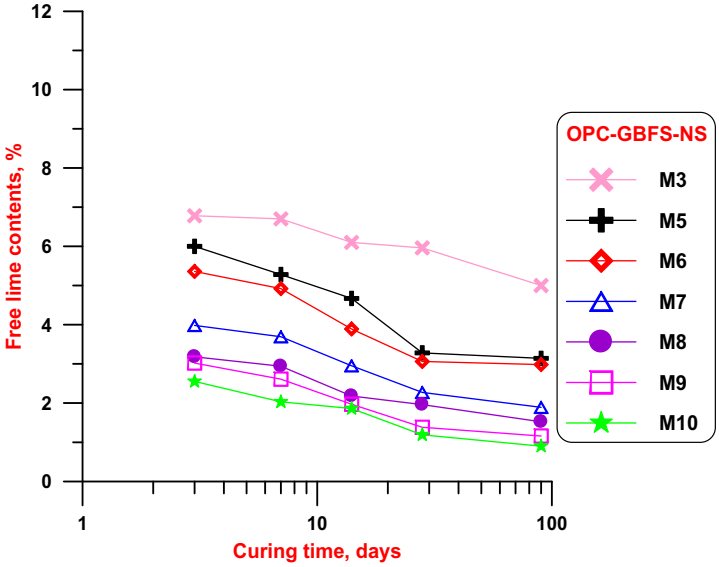

Fig. 15 Free lime contents of hydrated cement pastes as a function of curing time and nano-silica content.

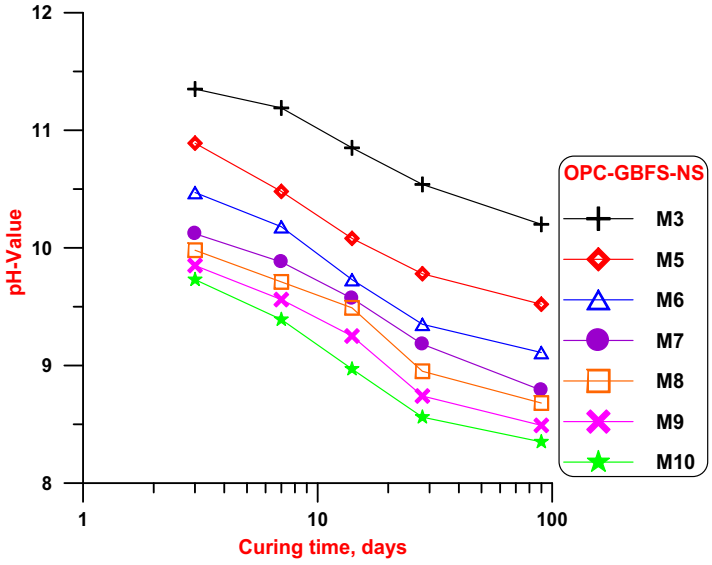

Fig. 16 pH-values of hydrated cement pastes with curing time and nanosilica content.

Mortars containing M7 and M8 (3–4% NS) possess higher values of compressive and flexural strengths and bulk density than those of the other mortars. This is attributed to the effect of NS, which behaves not only as a filler to improve microstructure, but also as an activator to promote pozzolanic reaction as well as acts as nucleating sites to form more accumulation and precipitation of calcium silicate, aluminate and alumino-silicate hydrates in the open pores originally filled with water, leading to the formation of homogeneous, dense and compact microstructure. By increasing the NS content than 4%, the bulk density and strength the increase of the resulting composite cements decrease but are still higher than those of M3 (OPC–GBFS). The effectiveness of NS in improving the compressive and flexural strengths and bulk density increases in the order: M3 < M5 < M6 < M10 < M9 < M7 < M8.

The effect of curing time up to 90 days on the hydration characteristics of M7 can be seen from XRD patterns shown in Fig. 20. XRD patterns show peaks of portlandite, CSH and $CaCO_3$ as well as anhydrous phases. The intensity of CSH peaks increases with increasing the age of the hydration, whereas the peaks corresponding to $Ca(OH)_2$ decreases with hydration age. This is attributed to two opposing processes; the first is continuous hydration reaction of cement phases (portlandite production), and the second is the pozzolanic reaction of NS with free portlandite, leading to the formation of excessive calcium silicate hydrates (lime capture). The peak intensity of $CaCO_3$ decreases with increasing hydration age due to the increased consumption of CH in the pozzolanic reaction of NS with the formation of additional amounts of CSH.

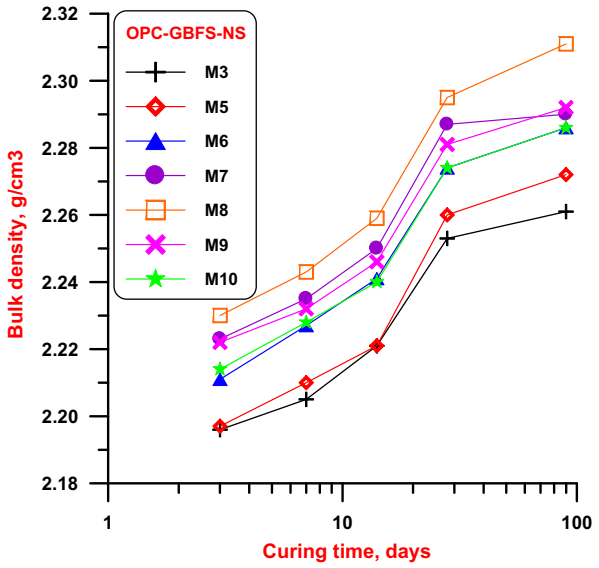

Fig. 17 Bulk density of hardened cement pastes containing nano-silica as a function of curing time up to 90 days.

Fig. 21 shows XRD patterns M0, M3, M6 and M7 hydrated for 28 days. Fig. 21 deposited the presence of anhydrous calcium silicate phases peaks superpose with the presence of hydrated phases such as CSH and $Ca(OH)_2$ peaks. OPC–GBFS–NS composite cement pastes (M6 and M7) exhibit lower intensity of portlandite peaks in comparison with those of M3, this is due the higher pozzolanic activity of NS than that of GBFS. Therefore, the rate of lime consumption and that of CSH production increase in the presence of NS.

Fig. 22 represents FTIR spectra of hydrated M7 composite cement paste as a function of curing time up to 90 days. The peak that appeared at 3640 cm^{-1} is due to the –OH group of $Ca(OH)_2$; its intensity decreases up to 90 days. The observed broad bands located at 3400 cm^{-1} and 1640–1650 cm^{-1} are due to stretching and bending vibrations of water bound to the hydrated silicates. The band around 1475 cm^{-1} is attributed to C–O bond stretching of CO_3^{2-}. The band that appeared in the range of 950–980 cm^{-1} is assigned to the formation of tobermorite like phase (CSH) [67].

FTIR spectra of cement pastes containing different NS contents hydrated for 28 days are shown in Fig. 23. It is well known that, the phases of non-ordered structures exhibit

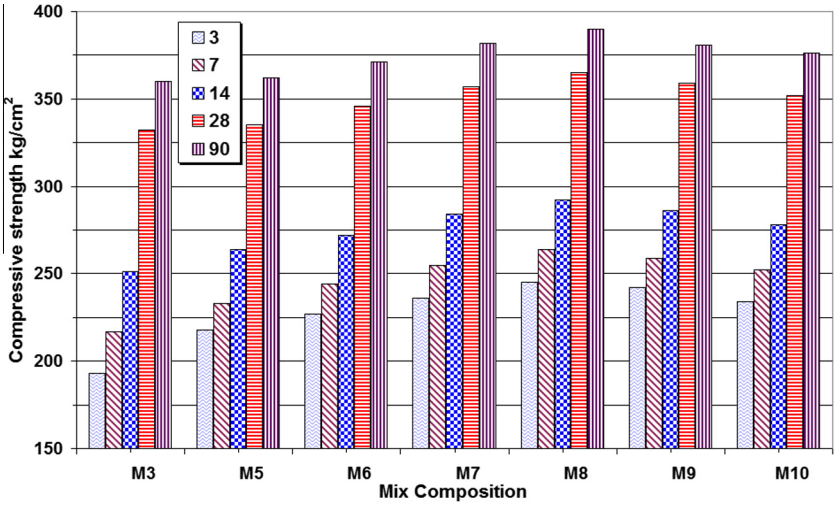

Fig. 18 Compressive strength of hardened cement mortars containing nano-silica with curing time up to 90 days.

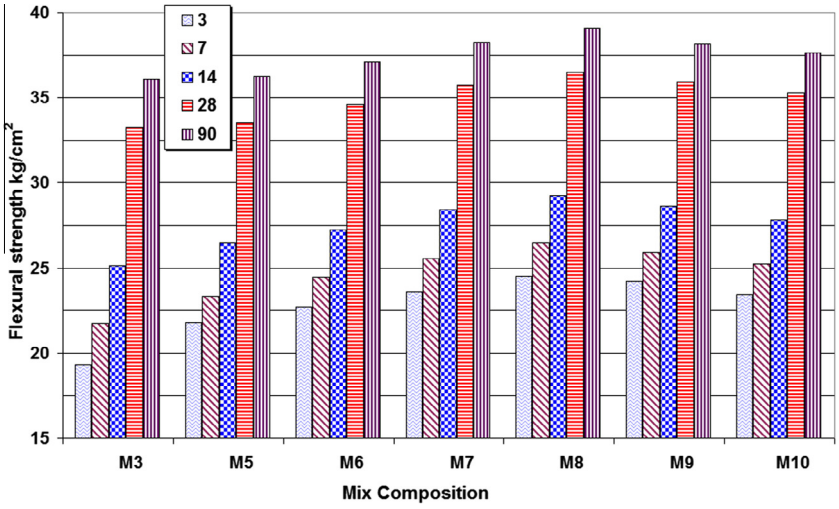

Fig. 19 Flexural strength of hardened cement mortars containing NS with curing time up to 90 days.

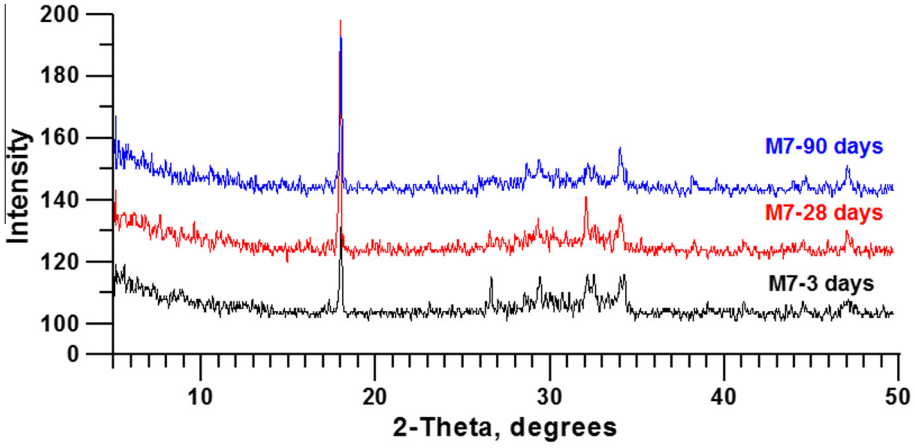

Fig. 20 XRD patterns of OPC–GBFS cement pastes containing NS hydrated for 90 days.

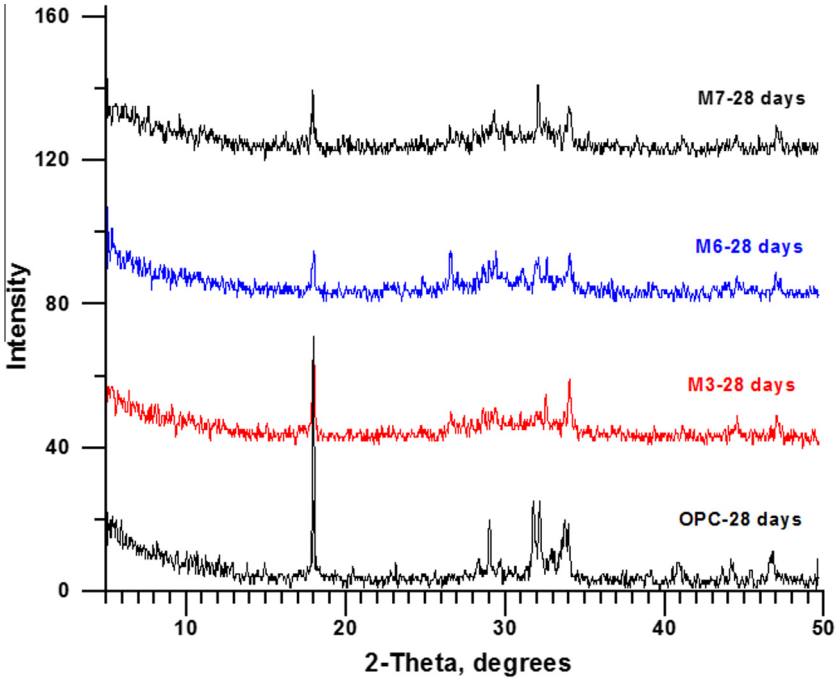

Fig. 21 XRD patterns of cement pastes containing NS hydrated for 28 days.

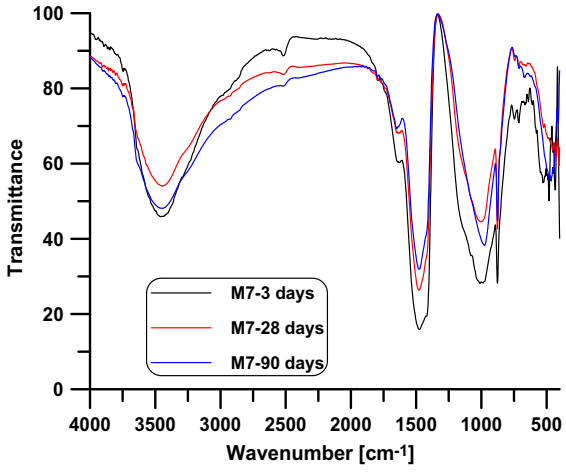

Fig. 22 FTIR spectra of M7 hydrated at different times.

broad bands with lower intensity in comparison with those of crystalline structures. The results show that, the peak intensity of –OH group from portlandite phase decreases with NS content, due to pozzolanic reaction of NS with the free lime liberated from OPC hydration. But, the peaks related to the stretching and bending vibrations of lattice water in the hydrated silicates and alumino-silicates (CSH and CASH) behave in opposite manner to that of portlandite; their intensities increase with NS content [70].

Fig. 24 represents the DSC thermograms of M7 hydrated for 90 days. It can be seen that, the intensity of the portlandite peak decreases up to 90 days. The endothermic peak corresponding to CSH has opposite manner to that of portlandite, because more $Ca(OH)_2$ consumption means more CSH production. The characteristic peak of calcite increases with hydration age up to 28 days and then decreases; the nano-particles promote the early hydration stages of cement phases with higher rate than the later ones.

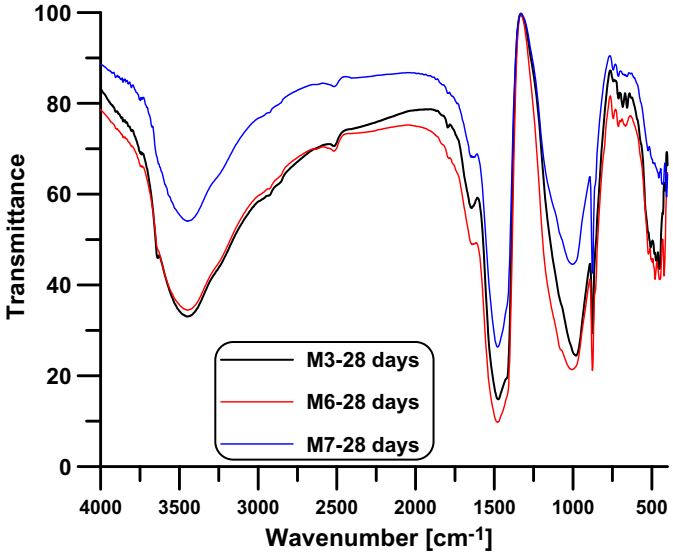

Fig. 23 FTIR spectra of different mixes hydrated at 28 days.

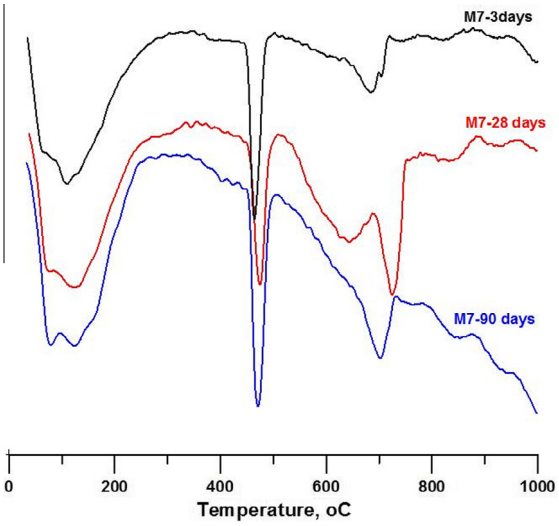

Fig. 24 DSC thermograms of M7 with curing times up to 90 days.

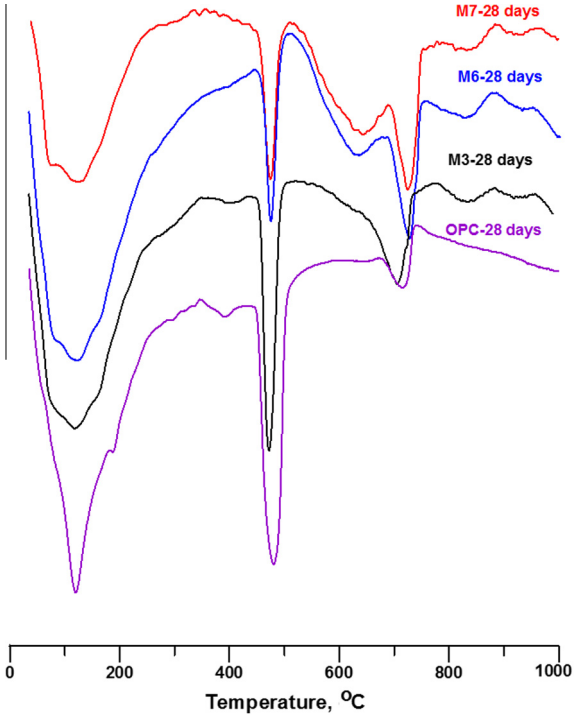

Fig. 25 DSC thermograms of different mixes hydrated at 28 days.

The DSC thermograms of hydrated OPC (M0), OPC–GBFS (M3) and OPC–GBFS–NS (M6 and M7) cement pastes hydrated for 28 days are shown in Fig. 25. The results show that the endothermic peak corresponding to CSH of OPC has lower intensity than those of OPC–GBFS–NS cement pastes. This is mainly due to the pozzolanic reaction of NS with the liberated lime during cement hydration, with the production of additional hydrated CSH products. Also, the endothermic peak of CSH increases with increasing NS content in the ascending order: M3 < M6 < M7. The endothermic peak area due to the decomposition of $Ca(OH)_2$ decreases with increasing NS content. The results of DSC thermograms are in good agreement with those of XRD, IR and chemical analysis.

Conclusions

The following conclusions can be derived from the results obtained in this study:

1. The required water of consistency decreases and setting times are elongated with increasing slag content in the OPC–GBFS blends.
2. The combined values of water content of OPC–GBFS are lower than those of OPC, especially at early hydration ages. But, at later ages, OPC–GBFS containing 30

and 45 mass% of GBFS possess higher W_n contents than those of OPC.

3. The values of free lime and pH decrease with the increase of curing time and GBFS content of OPC–GBFS blends.
4. As the GBFS content increases up to 45 mass% of OPC–GBFS mixes the bulk density, compressive and flexural strengths increase at later curing times.
5. The water demand and setting times of OPC–GBFS–NS increase with NS content; this is due to the retardation of the setting in the presence of 1% of superplasticizer.
6. As the nano-SiO_2 content of OPC–GBFS–NS increases the values of both FL and pH decrease.
7. The compressive and flexural strengths of OPC–GBFS–NS cement mortars containing NS are higher than those of OPC–GBFS control mix (M3). Above 4 mass% NS, the values of bulk density, compressive and flexural strengths decrease but are still more than those of the blank (M3).
8. The composite cements containing 45 mass% of GBFS and 3–4 mass% of NS give the optimum mechanical properties.

References

[1] G.A. Blengini, T. Di Carlo, The changing role of life cycle phases, subsystems and materials in the LCA of low energy buildings, Energy Build. 42 (6) (2010) 869–880.

[2] C. Becchio, S.P. Corgnati, A. Kindinis, S. Pagliolico, Improving environmental sustainability of concrete products: investigation on MWC thermal and mechanical properties, Energy Build. 41 (11) (2009) 1127–1134.

[3] N.B. Singh, B. Middendorf, Chemistry of blended cements part-I: natural pozzolanas, fly ashes and granulated blast furnace slags, Cem. Inter. 6 (4) (2008) 76–91.

[4] N.B. Singh, B. Middendorf, Chemistry of blended cements part-II: silica fume, metakaolin, reactive ashes from agricultural wastes, inert materials and non-Portland blended cements, Cem. Inter. 6 (2009) 78–93.

[5] K. Mukesh, S.K. Singh, N.P. Singh, N.B. Singh, Hydration of multicomponent composite cement: OPC–FA–SF–MK, Constr. Build. Mater. 36 (2012) 681–686.

[6] C. Shi, J. Qian, High performance cementing materials from industrial slags: a review, Resour. Conserv. Recycl. 29 (2000) 195–207.

[7] A. Nazari, S. Riahi, Splitting tensile strength of concrete using ground granulated blast furnace slag and SiO_2 nano-particles as binders, Energy Build. 43 (2011) 864–872.

[8] M.A. Smith, The economic and environmental benefits of increased use of pfa and granulated slag, Resour. Policy 1 (3) (1975) 154–170.

[9] C. Li, H. Sun, L. Li, A review: the comparison between alkali-activated slag (Si + Ca) and metakaoline (Si + Al) cements, Cem. Concr. Res. 40 (2010) 1341–1349.

[10] Chen W. Hydration of slag cement: theory, modeling and application. PhD Thesis, University of Twenty; 2007.

[11] R. Siddique, Waste Materials and By-Products in Concrete, Springer-Verlag, Berlin (Heidelberg), 2008.

[12] M. Regourd, Slags and Slag Cements. Concrete Technology and Design Cement Replacement Materials, Vol. 31, Guide Ford, Surrey Univ. Press, France, 1986, pp. 73–99.

[13] S. Kumar, R. Kumar, A. Bandopadhyay, T.C. Alex, B.R. Kumar, S.K. Das, S.P. Mehrotra, Mechanical activation of granulated blast-furnac slag and its effect on the properties and structure of Portland slag cement, Cem. Concr. Compos. 30 (2008) 679–685.

[14] B. Kolani, L.B. Lacarrière, A. Sellier, G. Escadeillas, L. Boutillon, L. Linger, Hydration of slag-blended cements, Cem. Concr. Compos. 34 (2012) 1009–1018.

[15] N.Y. Mostafa, Influence of air-cooled slag on physicochemical properties of autoclaved aerated concrete, Cem. Concr. Res. 35 (2005) 1349–1357.

[16] Q. Wang, P. Yan, G. Mi, Effect of blended steel slag–GBFS mineral admixture on hydration and strength of cement, Constr. Build. Mater. 35 (2012) 8–14.

[17] J.I. Escalante, L.Y. Gomez, K.K. Johal, G. Mendoza, H. Mancha, J. Mendez, Reactivity of blast-furnace slag in Portland cement blends hydrated under different conditions, Cem. Concr. Res. 31 (2001) 1403–1409.

[18] T. Saeki, P.J.M. Monteiro, A model to predict the amount of calcium hydroxide in concrete containing mineral admixtures, Cem. Concr. Res. 35 (2005) 1914–1921.

[19] F. Pacheco-Torgal, S. Jalali, Nanotechnology: advantages and drawbacks in the field of construction and building materials, Constr. Build. Mater. 25 (2011) 582–590.

[20] L. Senff, D.M. Tobaldi, S. Lucas, D. Hotza, V.M. Ferreira, J.A. Labrincha, Formulation of mortars with nano-SiO2 and nano-TiO2 for degradation of pollutants in buildings, Composites Part B 44 (2013) 40–47.

[21] Z. Bittnar, P.J.M. Bartos, J. Zeman, Nanotechnology in construction 3, in: Proceedings of the NICOM3, Springer, Berlin, 2009.

[22] L. Raki, J.J. Beaudoin, R. Alizadeh, J. Makar, T. Sato, Cement and concrete nanoscience and nanotechnology, Materials 3 (2010) 918–942.

[23] B.W. Jo, C.H. Kim, G.H. Tae, J.B. Park, Characteristics of cement mortar with nano-SiO_2 particles, Constr. Build. Mater. 21 (6) (2007) 1351–1355.

[24] M. Aiu, The Chemistry and Physics of Nano-Cement, Loyola Marymount University, NSF-REU University of Delaware, 2006.

[25] M.P. Ginebra, F.C.M. Driessens, J.A. Planell, Effect of the particle size on the micro and nano structural features calcium phosphate cement: a kinetic analysis, Biomaterials 25 (2004) 3453–3462.

[26] H. Li, H. Gang, X. Jie, J. Yuang, J. Ou, Microstructure of cement mortar with nanoparticles, Composites Part B 35 (2004) 185–189.

[27] Wilson M, Smith KKG, Simmons M, Raguse B. Nanotechnology-Basic Science and Emerging Technologies. Chapman & Hall/CRC; 2000.

[28] K. Sobolev, Engineering of SiO2 nano-particles for optimal performance in nano cement-based materials, in: Z. Bittnar, P.J.M. Bartos, J. Nemecek, V. Smilauer, J. Zeman (Eds.), Nanotechnology in Construction, Proceedings of the NICOM3, Prague, 2009, pp. 139–148.

[29] G Quercia, HJH. Brouwers, Application of Nano-Silica in Concrete Mixtures, 8th PhD Symposium in Kgs, Lyngby Denmark, 2010.

[30] A. Porro J.S. Dolado, I. Campillo, E. Erkizia, Y.de. Miguel, Saez.de.Y. Ibara, Effects of nano-silica additions on cement pastes, in:R.K. Dhir, M.D. Newlands, L.J. Csetenyi (Eds.), Proceedings of Applications of Nanotechnology in Concrete Design, 2005, pp. 87–96.

[31] Collepardi M, Collepardi S, Skarp U, Troli R. Optimization of silica fume, fly ash and amorphous nano-silica in superplasticized high-performance concretes, Proceedings of 8th CANMET/ACI International Conference on Fly Ash, Silica Fume, Slag and Natural Pozzolan in Concrete SP 221 USA, (2004); 495–506.

[32] L. Senff, D. Hotza, Mortars with nano-SiO_2 and micro-SiO_2 investigated by experimental design, Constr. Build. Mater. 24 (2010) 1432–1437.

[33] L. Senff, J.A. Labrincha, V.M. Ferreira, D. Hotza, W.L. Repette, Effect of nano-silica on rheology and fresh properties of cement pastes and mortars, Constr. Build. Mater. 23 (2009) 2487–2491.

[34] I. Zyganitidis, M. Stefanidou, N. Kalfagiannis, S. Logothetidis, Nano-mechanical characterization of cement-based pastes enriched with SiO_2 nano-particles, Mater. Sci. Eng., B 176 (9) (2011) 1580–1584.
[35] Lee BY, Thomas JJ, Treager M, Kurtis KE. Influence of TiO2 Nano-particles on Early C3S Hydration, Nanotechnology of Concrete. The Next Big Thing is Small, ACI editors: Konstantin S, Taha MR, SP-267- 4; 2009.
[36] Metaxa ZS, Konsta-Gdoutos MS, Shah SP. Carbon nano-tubes Reinforced Concrete, Nanotechnology of Concrete: The Next Big Thing is Small, ACI editors: Konstantin S, Taha MR., SP-267-2; 2009.
[37] M. Oltulu, R. Sahin, Single and combined effects of nano-SiO_2, nano-Al_2O_3 and nano-Fe_2O_3 powders on compressive strength and capillary permeability of cement mortar containing silica fume, Mater. Sci. Eng., A 528 (2011) 7012–7019.
[38] Ge Z, Gao Z. Applications of Nanotechnology and Nanomaterials in Construction. 1st Inter Confer Constr Developing Countries (ICCIDC-I), Advancing and Integrating Construction Education, Research & Practice, Karachi, Pakistan, August 4–5; 2008.
[39] S. Hanehara, M. Ichikawa, Nanotechnology of cement and concrete, J. Taiheiyo Cem. Corp. 141 (2001) 47–58.
[40] K.L. Scrivener, Nanotechnology and cementitious materials, in: Z. Bittnar, P.J.M. Bartos, J. Nemecek, V. Smilauer, J. Zeman (Eds.), Nanotechnology in Construction: Proceedings of the NICOM3; 3rd International Symposium on Nanotechnology in Construction, Czech Republic, Prague, 2009, pp. 37–42.
[41] K. Sobolev, S.P. Shah, Nanotechnology of Concrete: Recent Developments and Future Perspectives, American Concrete Institute, Detroit, 2008, SP-254.
[42] P.J.M. Bartos, Y. de Miguel, A. Porro (Eds.), NICOM: 2nd International Symposium on Nanotechnology for Construction, RILEM Publications SARL, Bilbao, Spain, 2006.
[43] Z. Bittnar, P.J.M. Bartos, J. Nemecek, V. Smilauer, J. Zeman (Eds.), Nanotechnology in Construction: Proceedings of the NICOM3 (3rd International Symposium on Nanotechnology in Construction), Springer-Verlag Berlin Heidelberg, Prague, Czech Republic, 2009, p. 438.
[44] K. Sobolev, M. Ferrada-Gutierrez, How nanotechnology can change the concrete World: Part 1, Am. Ceram. Soc. Bull. 10 (2005) 14–17.
[45] G. Li, Properties of high-volume fly ash concrete incorporating nano-SiO_2, Cem. Concr. Res. 34 (2004) 1043–1049.
[46] A. Nazari, S. Riahi, The effects of SiO_2 nanoparticles on physical and mechanical properties of high strength compacting concrete, Compos. Part., B Eng. 42 (2011) 570–578.
[47] Y. Qing, Z. Zenan, S. Li, C. Rongshen, A comparative study on the pozzolanic activity between nano-SiO_2 and silica fume, J. Wuhan Univ. Technol., Mater. Sci. Ed. 21 (3) (2008) 153–157.
[48] H.M. Jennings, J.W. Bullard, J.J. Thomas, J.E. Andrade, J.J. Chen, G.W. Scherer, Characterization and modeling of pores and surfaces in cement paste: correlations to processing and properties, J. Adv. Concr. Technol. 6 (1) (2008) 5–29.
[49] Y. Qing, Z. Zenan, K. Deyu, C. Rongshen, Influence of nano-SiO_2 addition on properties of hardened cement paste as compared with silica fume, Constr. Build. Mater. 21 (2007) 539–545.
[50] K.L. Lin, W.C. Chang, D.F. Lin, H.L. Luon, M.C. Tsai, Effects of nano-SiO_2 and different ash particle sizes on sludge ash–cement mortar, J. Environ. Manage. 88 (2008) 708–714.
[51] T. Ji, Preliminary study on the water permeability and microstructure of concrete incorporating nano-SiO_2, Cem. Concr. Res. 35 (10) (2005) 1943–1947.
[52] A. Nazari, Sh. Riahi, Microstructural, thermal, physical and mechanical behavior of the self compacting concrete containing SiO_2 nanoparticles, Mater. Sci. Eng., A 527 (2010) 7663–7672.
[53] J. Björnström, A. Martinelli, A. Matic, L. Börjesson, I. Panas, Accelerating effects of colloidal nano-silica for beneficial calcium–silicate–hydrate formation in cement, Chem. Phys. Lett. 392 (2004) 242–248.
[54] M.A. Abd-El-Eziz, M. Heikal, Hydration characteristics and durability of cements containing fly ash and limestone subjected to Qaron's Lake Water, Adv. Cem. Res. 21 (3) (2009) 91–99.
[55] ASTM Designation, C191, Standard method for normal consistency and setting of hydraulic cement, ASTM Annual Book of ASTM Standards, 2008.
[56] M. Abd-El Aziz, S. Abd El Aleem, M. Heikal, Physico-chemical and mechanical characteristics of pozzolanic cement pastes and mortars hydrated at different curing temperatures, Constr. Build. Mater. 26 (2012) 310.
[57] H. El-Didamony, M. Abd-El Eziz, S. Abd El Aleem, M. Heikal, Hydration and durability of sulfate resisting and slag cement blends in Qaron's Lake water, Cem. Concr. Res. 35 (2005) 1592–1600.
[58] H. El-Didamony, M. Heikal, S. Abd El Aleem, Influence of delayed addition time of sodium sulfanilate phenol formaldehyde condensate on the hydration characteristics of sulfate resisting cement pastes containing silica fume, Constr. Build. Mater. 37 (2012) 269–276.
[59] ASTM C109, Strength test method for compressive strength of hydraulic cement mortars, 2007.
[60] V.S. Ramachandran, Thermal Analysis, in: V.S. Ramachandran, J.J. Beaudoin (Eds.), Handbook of Analytical Techniques in Concrete Science and Technology, Noyes publications, New Jersey, 2001, pp. 147–149, ISBN: 0-8155.
[61] R.J. Errington, Advanced Practical Inorganic and Metalorganic Chemistry, Blackie Academic & Professional, An Imprint Chapman & Hall, 1997.
[62] Mehta PK. 3rd International Conference on Fly Ash, Silica Fume, Natural Pozzolan in Concrete, Relim Tronheim, Norway, 1989:1–43.
[63] V.M. Maihotra, Properties of Fresh and Hardened Concrete Incorporating Ground Granulated Blast Furnace Slag, in: V.M. Malhotra (Ed.), Supplementary cementing materials for concrete, Canadian Government Publishing Centre, Ottawa, 1987, pp. 291–331.
[64] H.F.W. Taylor, Cement Chemistry, 2nd ed., London, Thomas Telford Publishing, 1997.
[65] J.M. Khatib, J.J. Hibbert, Selected engineering properties of concrete incorporating slag and metakaoline, Constr. Build. Mater. 19 (6) (2005) 460–472.
[66] Bensted J. Applications of Infrared Spectroscopy to cement hydration. Construction materials group and institute of materials meeting on techniques for characterization of cement hydration, London; Society of Chemical Industry, 1994.
[67] A.H. Delgado, R.M. Paroli, J.J. Beaudoin, Comparison of IR techniques for the characterization of construction cement minerals and hydrated products, Appl. Spectrosc. 50 (8) (1996) 970–976.
[68] C. Legrand, E. Wirquin, Study of the strength of very young concrete as a function of the amount of hydrates formed-influence of superplasticizer, Mater. Struct. 166 (1994) 106–109.
[69] H. Li, M. Zhang, J. Ou, Flexural fatigue performance of concrete containing nanoparticles for pavement, Int. J. Fatigue 29 (2007) 1292–1301.
[70] X.F. Gao, Y. Lo, C.M. Tam, C.Y. Chung, Analysis of the infrared spectrum and microstructure of hardened cement paste, Cem. Concr. Res. 29 (1999) 805–812.